Thinning Segregated Graphene Layers on High Carbon Solubility Substrates of Rhodium Foils by Tuning the Quenching Process

Mengxi Liu,[†] Yanfeng Zhang,[†,‡,*] Yubin Chen,[†] Yabo Gao,[†] Teng Gao,[†] Donglin Ma,[†] Qingqing Ji,[†] Yu Zhang,[†,‡] Cong Li,[†] and Zhongfan Liu[†,*]

[†]Center for Nanochemistry (CNC), Beijing National Laboratory for Molecular Sciences, State Key Laboratory for Structural Chemistry of Unstable and Stable Species, College of Chemistry and Molecular Engineering and [‡]Department of Materials Science and Engineering, College of Engineering, Peking University, Beijing 100871, People's Republic of China

ABSTRACT We report the synthesis of large-scale uniform graphene films on high carbon solubility substrates of Rh foils for the first time using an ambient-pressure chemical vapor deposition method. We find that, by increasing the cooling rate in the growth process, the thickness of graphene can be tuned from multilayer to monolayer, resulting from the different segregation amount of carbon atoms from bulk to surface. The growth feature was characterized with scanning electron microscopy, Raman spectra, transmission electron microscopy, and scanning tunneling microscopy. We also find that bilayer or few-layer graphene prefers to stack deviating from the Bernal stacking geometry, with the formation of versatile moiré patterns. On the basis of these results, we put forward a segregation growth mechanism for graphene growth on Rh foils. Of particular importance, we propose that this randomly stacked few-layer graphene can be a model system for exploring some fantastic physical properties such as van Hove singularities.

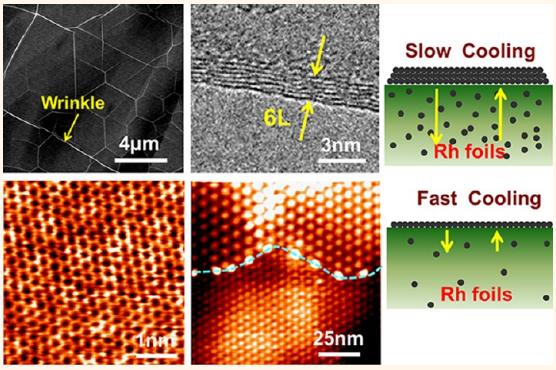

KEYWORDS: graphene · APCVD · moiré pattern · STM · wrinkle

Graphene, being the hexagonal arrangement of carbon atoms, has attracted vast interest since it was isolated in 2004 for its remarkable physical and chemical properties,[1] such as quantum Hall effects,[2] high carrier mobility[1,3,4] (up to 200 000 $cm^2 V^{-1} s^{-1}$), and perfect optical transparency.[5,6] Recently, it was reported that when increasing the layer thickness from monolayer to few layers, the physical properties of graphene can be dramatically modulated. Bernal-stacked bilayer graphene presents a tunable band gap up to 250 mV by an external electric field,[7−11] while non-Bernal bilayer graphene demonstrates van Hove singularities (VHSs) in the density of states which may lead to new phases of matter.[12] Trilayer graphene exhibits spin−orbit interaction (SOI) which provides the possibility to electrically manipulate spin precession in graphene systems without ferromagnetics.[13] Moreover, few-layer graphene possesses broad applications in electronics,[14] capacitors, and so on.[15,16]

Preparations of graphene layers with controllable thickness, large domain size, and different stacking orders are the premise of such studies. Until now, Cu foils, with nearly negligible carbon solubility at the temperature to growth, are the most widely used substrates for growing large-scale uniform monolayer graphene.[5,17−19] A self-limited growth mechanism is proposed, due to the high catalytic capability of Cu, which inhibits the formation of perfect bilayer and few-layer films. In contrast, Ni films, owing a high carbon solubility of 0.9 atom % at 1000 °C, served as another commonly used substrate to grow graphene, with the thickness variable from monolayer to dozens of layers

* Address correspondence to yanfengzhang@pku.edu.cn, zfliu@pku.edu.cn.

Received for review July 19, 2012 and accepted November 16, 2012.

Published online November 17, 2012
10.1021/nn3047154

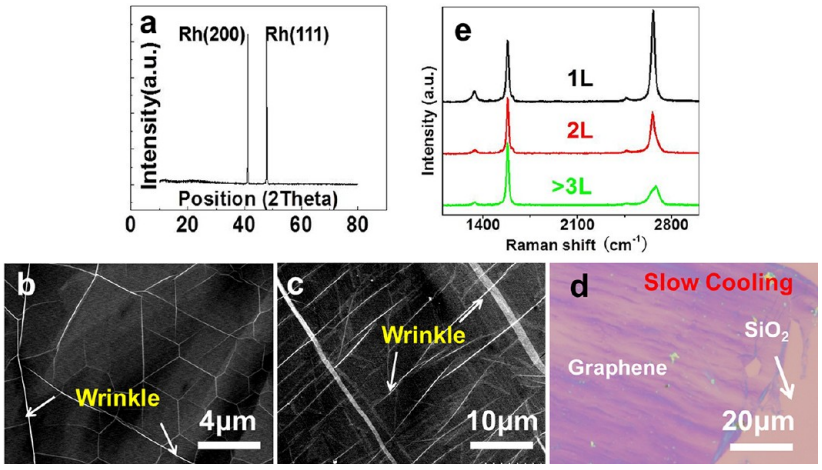

Figure 1. Characterizations of graphene growth on Rh foils under slow cooling process (15 °C/min). (a) XRD pattern of the sample. (b,c) SEM images of the sample. (d) OM image after being transferred onto SiO_2/Si. (e) Corresponding Raman spectra of (d) showing multilayer (*n*L) films along with a little portion of 1L and 2L regions, under a Raman excitation wavelength of 633 nm.

by changing the growth temperature, growth time, or quenching rate,[6,14,20−27] and segregation of carbon from bulk Ni to the surface is thought to be the possible channel for graphene growth. However, although many experimental efforts have been tried, on the well-known Ni substrate, controllable growth from monolayer to few-layer graphene with high thickness uniformity is still a huge challenge.

Besides polycrystalline Cu and Ni, the graphene growth on noble metals was also intensively investigated, while limited to single-crystal substrates and under ultrahigh vacuum (UHV) growth conditions.[28−41] For example, high-quality monolayer graphene growth on Rh(111) was realized at 600 °C under UHV conditions.[40−44] This kind of graphene sample, usually having a size of 1 cm^2, usually serves as a model system for investigating the atomic-scale structure and the electronic property of graphene with the aid of scanning tunneling microscopy (STM). By intuition, polycrystalline Rh could be another choice for preparing graphene.

In this paper, we report the growth of graphene on Rh foils using an ambient-pressure chemical vapor deposition (APCVD) method. By virtue of scanning electron microscopy (SEM), transmission electron microscopy (TEM), Raman spectra, and STM, we characterized the morphology, layer thickness, and stacking order of the graphene samples. We then explored the probability of controlling the graphene layer thickness by altering the growth parameters, especially by adjusting the quenching rate in the CVD process. Finally, we discussed the growth mechanism of graphene on Rh foils and compared it with its analogue system of graphene on polycrystalline Ni films.

RESULTS AND DISCUSSION

We use the APCVD method to grow graphene on Rh foils rather than low-pressure CVD (LPCVD). This is because the growth by LPCVD usually results in diverse graphene flakes but not complete layers, even if the growth parameters, such as the flow rate of CH_4 and the growth time, were tuned to a large extent (see Supporting Information Figure S1). This phenomenon indicates that the LPCVD method cannot provide enough carbon sources to form complete graphene films on Rh foils.

Graphene samples of Figures 1−4 were initially prepared through a traditional CVD process (see Supporting Information Figure S2), under a slow cooling rate of 15 °C/min. First, we used X-ray diffraction (XRD) to obtain the facets of Rh after CVD growth. Figure 1a shows (111) and (200) facets of Rh possessing almost equal diffraction intensities. Second, we carried out SEM examinations to see the surface morphology of graphene on Rh foils. The surface is characterized with a dark background and some stripped bright interconnecting lines, which correspond to graphene and graphene wrinkles, respectively. The wrinkles usually encircling into nearly hexagonal (Figure 1b) or quadrilateral (Figure 1c) shapes may reflect a strong substrate facet symmetry effect, and this issue will be discussed in Figure 4.[45]

It is noteworthy that Rh is hard to dissolve in ordinary acids, even in aqua regia. In this case, we utilized an improved bubble method to fulfill a scatheless transfer of the sample.[46] The unique trait of this method is that a cyclic use of Rh foils can be realized with graphene, avoiding metallic ion pollution. The optical microscopy (OM) image of the sample after being transferred onto 300 nm SiO_2/Si substrates is demonstrated in Figure 1d. According to the contrast difference, the film is mainly composed of multilayer graphene (purple contrast) and a small portion of few-layer graphene (pink contrast).[47]

We then performed Raman spectroscopy to reconfirm the thickness distributions (Figure 1e). We found

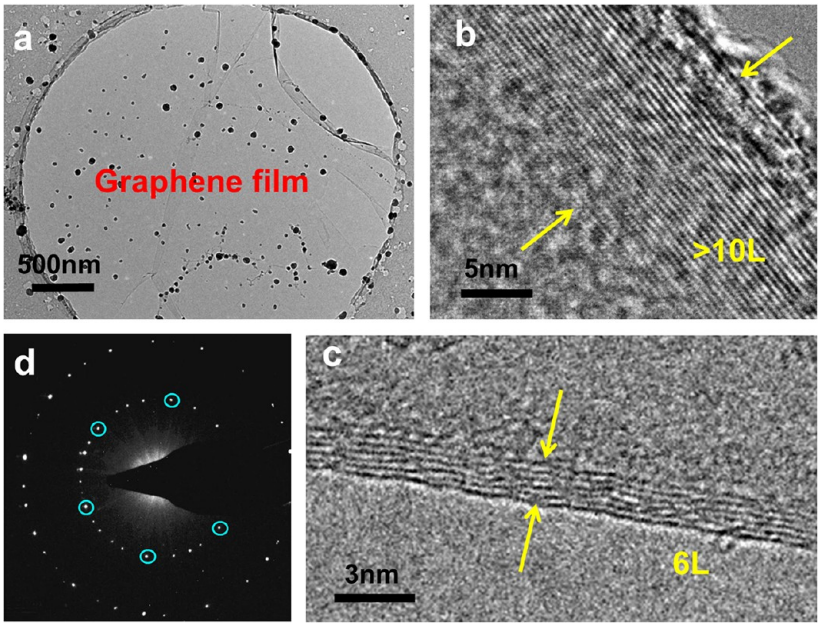

Figure 2. TEM images of graphene grown with a slow cooling process. (a) Low-magnification image of continuous graphene films. (b,c) HRTEM images of the folded regions showing explicit layer numbers. (d) Selected area electron diffraction (SAED) pattern taken from the center of the graphene domain in (a) (encircled dots represent one set of electron diffraction patterns).

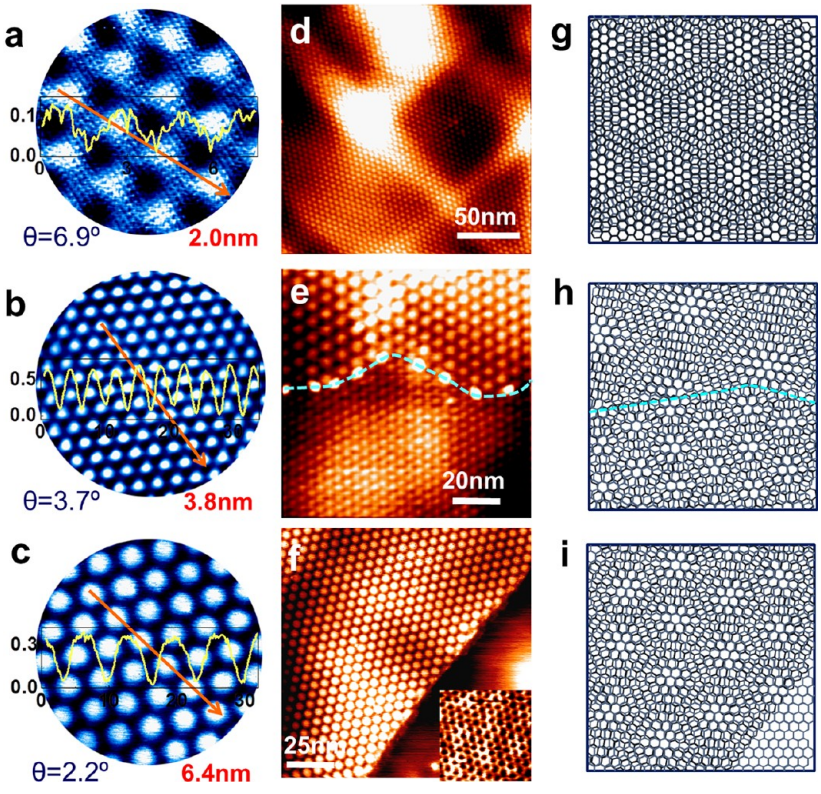

Figure 3. (a–c) STM images of rotated graphene layers with the formation of various moiré patterns. The inserted height profiles along the indicated lines reveal the roughness of the moirés: (a–c) θ = 6.9, 3.7, 2.2°; D = 2.0, 3.8, 6.4 nm (V_T = −0.002, −0.002, −0.002 V; I_T = 39.67, 2.27, 2.27 nA). (d) Large-scale STM image of graphene with only one set of moiré pattern (200 nm × 200 nm; V_T = −0.229 V, I_T = 4.29 nA). (e) Two top graphene flakes rotated differently with respect to the underneath layer exhibiting different moiré patterns with obvious point defects along the linking edge (86 nm × 86 nm; V_T = −0.022 V, I_T = 1.36 nA). (f) Smaller graphene patch covered by a larger layer (200 nm × 200 nm; V_T = −0.002 V, I_T = 2.66 nA). The right bottom inset is an atom-scale resolution STM image of the right bottom corner, showing hexagonal lattices revealing its monolayer nature (2 nm × 2 nm; V_T = −0.062 V, I_T = 4.29 nA). (g–i) Schematic drawings of (d–f).

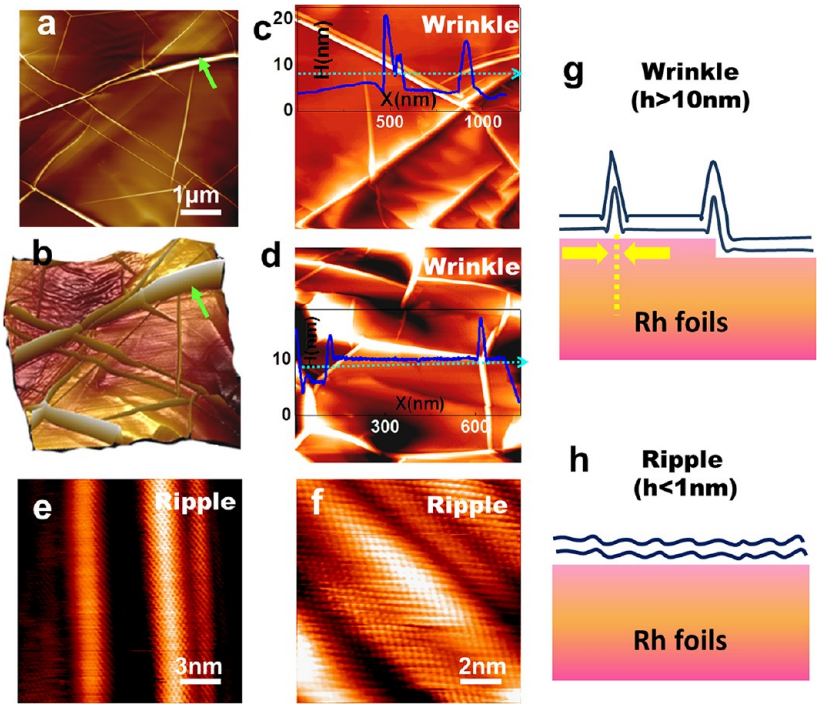

Figure 4. (a,b) AFM image and its 3D contour showing the formation of graphene wrinkles along the Rh grain boundaries. (c, d) Corresponding large-scale STM images and their height profiles along the line directions: (c) 1200 nm × 1200 nm; V_T = −1.162 V, I_T = 4.29 nA; (d) 800 nm × 800 nm; V_T = −0.53 V, I_T = 4.89 nA. Wrinkles can also evolve along the step edge of a single facet. (e,f) Atomically resolved images on ripple surfaces: (e) 10 nm × 10 nm; V_T = −0.010 V, I_T = 1.94 nA; (f) 15 nm × 15 nm; V_T = −0.006 V, I_T = 1.66 nA. (g,h) Schematic drawings of wrinkle and ripple formation.

that monolayer (black line), bilayer (red line), and more than bilayer (green line) Raman signals can be obtained using a 633 nm laser. The D bands of the spectra (~1340 cm^{-1}), corresponding to defect states in graphene, are negligible and almost vanish with increasing graphene thickness, indicative of nearly defect-free graphene. On the rarely occurring thinner regions, the spectra show an intensity ratio of the 2D band at ~2680 cm^{-1} to G band at ~1584 cm^{-1} close to 2 and 1, and the full width at half-maximum (fwhm) values of 2D bands are 30 and 45 cm^{-1}, respectively, in parallel with monolayer and bilayer formation. On the universally thicker appearing regions, I_{2D}/I_G is less than 0.5, and the fwhm of 2D bands is around 70 cm^{-1}, corresponding to multilayer graphene. In addition, Raman mapping was also carried out over a 20 μm × 20 μm area to verify the multilayer nature of the film (see Supporting Information Figure S3).

We use the same bubble method to transfer graphene films on TEM lacey carbon-coated grids (Figure 2a) to ensure the layer number by section-view analysis. Typically, we observe a large amount of multilayer (>10 layer) regions on most areas of our samples and a little portion of few-layer regions (<6L), as shown in Figure 2b,c, respectively, in coincidence with our OM and Raman mapping data. Electron diffraction patterns (Figure 2d) captured from Figure 2a usually reveal a pearl ring pattern, consisting of more than six sets of hexagonal patterns. This suggests randomly rotated stacking orders in the vertical direction of multilayer graphene, and there is no preferable rotation angle.

In this section, we examine the actual stacking geometry and the microscopic continuity of CVD graphene on Rh foils by high-resolution STM images. It is known that graphene moiré patterns, originating from the lattice constant mismatch between graphene and substrate or the relative rotation between adjacent graphene layers, can reveal their stacking orders. It was reported that graphene on Rh(111) prepared under UHV conditions has a triangular moiré periodicity of 2.88 nm, arising from a geometry of 12 × 12 C (a_C = 0.246 nm) on 11 × 11 Rh atoms (a_{Rh} = 0.269 nm), where a_C and a_{Rh} are the lattice constants of graphene and Rh, respectively.[41] In the APCVD system, graphene growth on Rh foils usually presents versatile moiré patterns in some thinner regions, which are proposed to arise from rotated stacking among few-layer graphene.

Figure 3a−c shows three typical STM images of such moiré patterns. The line profiles along the indicated lines display the heights and the periods of the moiré patterns. With the experimental data, we can use the following equation to calculate the rotation angle (θ) between two adjacent layers:

$$D = d/[2\sin(\theta/2)] \quad (1)$$

where d is the lattice constant of graphene (0.246 nm). According to eq 1, the relative rotation angles can be calculated to be 6.9, 3.7, and 2.2°, corresponding to

moiré periods of 2.0, 3.8, and 6.4 nm, respectively. More STM images of the moiré patterns are exhibited in Figure S4 in Supporting Information. Note that the domain size of single-crystalline graphene with a uniform moiré pattern can be as large as ~800 nm, as shown in Figure 3d. This is proposed to originate from two twisting graphene layers, with its schematic drawing shown in Figure 3g. With high-resolution STM images, we can also examine the linking type among different domains. In Figure 3e, two graphene domains with different orientations were jointed together over a complete layer (schematic drawing shown in Figure 3h), as proved by point defects along the linking edge. Figure 3f displays a moiré pattern in the top left corner, while the hexagonal lattice is shown in the bottom right corner parallel with monolayer graphene. Thus, a larger graphene flake riding over a smaller one is proposed for Figure 3f (schematic drawing shown in Figure 3i). The growth phenomenon may serve as a tentative proof for the segregation mechanism. On these twisted graphene layers, we found that two low-energy VHSs are induced with the energy difference (ΔE_{VHSs}) having an angle-dependent feature.[48] In this case, graphene on Rh foils provides an ideal platform for engineering the electronic states near the Fermi energy and the resulting attractive phases.

As mentioned above (Figure 1b,c), high-density graphene wrinkles, possibly affected by Rh(111) or Rh(200) facets, usually encircle into hexagonal or quadrilateral networks. These wrinkles are proposed to be a consequence of compressive stress during the quenching process because of the different thermal expansion coefficients of graphene and substrates. As the thermal expansion coefficient of graphite varies from -1.25×10^{-6}/K at 20 °C to 1.25×10^{-6}/K at 1000 °C, while the value of Rh changes from 7.86×10^{-6}/K to 13.65×10^{-6}/K at the same temperature range, this will induce a dramatic shrinking of the metal substrate and, in turn, the formation of graphene wrinkles.

Besides thermal expansion mismatch, substrate corrugation may also contribute to the wrinkle formation. For graphene on Rh foils, the growth temperature of graphene (1000 °C) is near the melting point of Cu (1084 °C) but far away from Rh (1960 °C). This disparity may induce a rather larger surface corrugation and a higher wrinkle density on Rh foils than that on Cu foils. In order to analyze the formation mechanism of wrinkles on Rh foil, we then captured atomic force microscopy (AFM) images of the sample (Figure 4a). From its 3D presentation (Figure 4b), it is clear that wrinkles are actually evolving along the step boundaries of Rh.

In order to establish a direct correlation of the position of the wrinkle and the substrate terrace, we then captured large-scale STM images in Figure 4c, presenting a wrinkle formation along the step boundary of Rh. The height profile recorded along the arrow exhibits a wrinkle height of ~15 nm over a lateral distance of ~70 nm. Wrinkles arranged into hexagonal shapes can also be observed in the STM image of Figure 4d, which evolves along the boundary of an isolated Rh grain.

According to many experimental facts, we can conclude that the wrinkle height is much higher than that on Ni films (~8 nm) and Cu foils (~3 nm).[45,49] Because of the high curvature of the wrinkle, we cannot achieve an atomically resolved STM image directly on the wrinkle surface. As a poignant contrast, we obtained an atomically resolved image on 0.5−1.0 nm high ripples (Figure 4e,f), which show clear graphene lattices.

In order to provide a visual image, the schematic drawings of wrinkle and ripple formation are demonstrated in Figure 4g,h. It is proposed that, since Rh foils are covered by graphene films completely, the stress due to thermal expansion mismatch contributes to the dominant factor for wrinkle formation, and wrinkles prefer to evolve along the highly corrugated regions such as step or facet boundaries. It was reported that along "folded wrinkles", anisotropy in their electrical resistivity usually occurs, leading to depressed device properties.[50] In this case, reducing the graphene wrinkle is of fundamental important for further improving the transport property of CVD graphene. Meanwhile, the ubiquitous graphene wrinkles on Rh foils with different wrinkle heights contribute a more ideal system for exploring the effects of graphene wrinkles on the local electronic properties.

As a result, graphene samples prepared through a moderate cooling process are mostly multilayers with random stacking geometries, which resemble graphene samples grown on Ni (with a carbon solubility of 0.9 atom % at 1000 °C). We expect that graphene grown on Rh foils may follow a segregation growth mechanism, considering the high carbon solubility of Rh (0.25 atom % at 1000 °C).[20,51] For equal carbon sources derived from the CVD process (under the same growth temperature and growth time), cooling rate becomes a key point to control carbon segregation quantity and velocity. Quickening the quenching rate probably takes effect on reducing carbon segregation and the layer thickness.

In our experiment, under a fast cooling process (150 °C/min), we obtain mostly monolayer and a few bilayer graphene films. The graphene films can also be transferred onto SiO_2 substrates by a bubble method. Large-scale OM image (Figure 5a) shows a uniform film over at least 100 μm × 100 μm with a pinkish purple color. Corresponding Raman spectra taken on the pinkish purple area are demonstrated in Figure 5b. The absence of a D band (~1350 cm^{-1}) indicates that the bubble method is also suitable for transferring ultrathin graphene films grown on Rh foil. With the intensity ratio of 2D band (~2650 cm^{-1}) to G band (~1584 cm^{-1}) ~1.2 and the fwhm of the 2D band

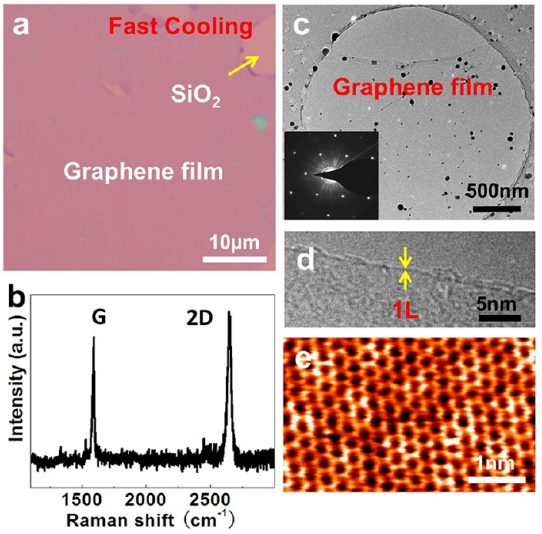

Figure 5. Graphene films grown on Rh foils through fast cooling process (150 °C/min). (a) OM image of the sample after being transferred onto SiO_2/Si. (b) Corresponding Raman spectra. (c) Low-magnification TEM image of the film, with an SAED pattern inset. (d) HRTEM image of the folded region in (c). (e) Atomically resolved STM image of graphene on Rh foils.

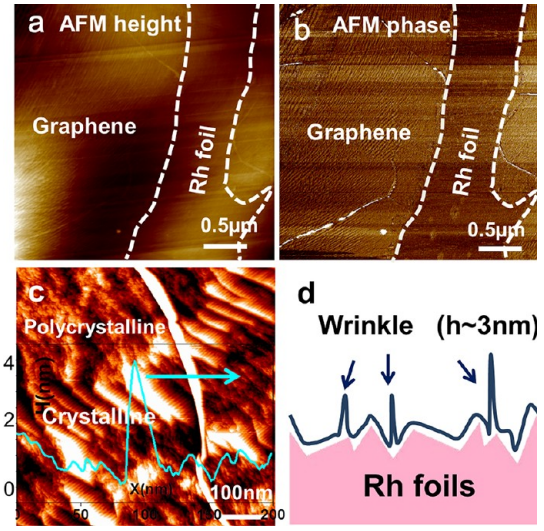

Figure 6. (a) AFM height image of graphene on the corrugated Rh foil (grown with a fast cooling process). (b) Corresponding AFM phase image showing graphene and bare Rh foils identified by their different contrasts. (c) Large-scale STM image of graphene on Rh foils. (d) Schematic drawing of wrinkle formation.

at 30 cm^{-1}, it is expected that we obtained mono- or bilayer graphene. TEM and SAED were also utilized to determine the layer number, as well as the stacking behavior of the graphene sample (Figure 5c). HRTEM images taken on the folded edge of Figure 5a shows the coexistence of mostly monolayer graphene films (Figure 5d). The SAED pattern (inset in Figure 5c) reveals a single set of hexagonal pattern, with the intensity ratio of the two outer peaks over the two inner peaks being ~0.5 (see Supporting Information Figure S5), authenticating its monolayer nature of the graphene. Moreover, atomically resolved STM images on most regions of the sample usually demonstrate hexagonal lattices (Figure 5e), reconfirming monolayer graphene formation. As a result, by increasing the cooling rate in the CVD process, the film thickness of graphene can be tunable from multilayer to monolayer.

For the monolayer samples, we find that, from AFM height images (Figure 6a), it is hard to recognize the regions of graphene and Rh, and even hard to identify graphene wrinkles. Alternatively, we conclude that the AFM phase image can recognize both regions (Figure 6b) where dark and bright regions represent Rh foil and graphene, respectively. In addition, we also utilized STM to explore the exact morphology of the sample. Figure 6c demonstrates the graphene growth on polycrystalline and crystalline Rh foils. A 3 nm high wrinkle, riding over the terraced and the amorphous regions, can be clearly identified from the inserted height profile analysis.

It is clear to see that the height, location, and density of wrinkles on monolayer graphene differ from that on multilayer graphene. This issue can be understood by the quenching process, where thermal expansion mismatch induced strain should be similarly released on monolayer graphene, leading to wrinkle formation. However, the corrugated substrate of Rh foils may accommodate part of the strain through graphene conforming to the undulated substrate, hereby leading to reduced wrinkle density (schematic drawing in Figure 6d).

On the basis of the high carbon solubility of Rh foils and the characteristics of graphene growth under different cooling rates, we propose a segregation mechanism for graphene on Rh foils under APCVD conditions (Figure 7a). To support this, the dissolution and segregation ability of carbon into Rh foils was also obtained by XPS depth measurement (see Supporting Information Figure S6). At 1000 °C, methane gases are decomposed on Rh foil surfaces for its perfect ability to catalyze hydrocarbon decomposition, and contemporary carbon atoms dissolve into bulk Rh because of its high carbon solubility.[51] In the cooling process of CVD growth, the solubility of carbon becomes lower with decreasing sample temperature, and therefore, excess carbon atoms would segregate from bulk to the surface, forming graphene layers.

Under slow cooling (Figure 7c,e), the growth process is dominated by a balance between dissolution and segregation of carbon, and in the relative long cooling process, carbon atoms have enough time to segregate to metal surfaces to form multilayer graphene. In contrast, under fast cooling (Figure 7b,d), the balance between dissolution and segregation of carbon is destroyed, and only a small amount of carbon can be segregated from bulk to the surface, leading to the formation of mainly monolayer graphene. This result is comparable with the graphene growth on Ni(111),

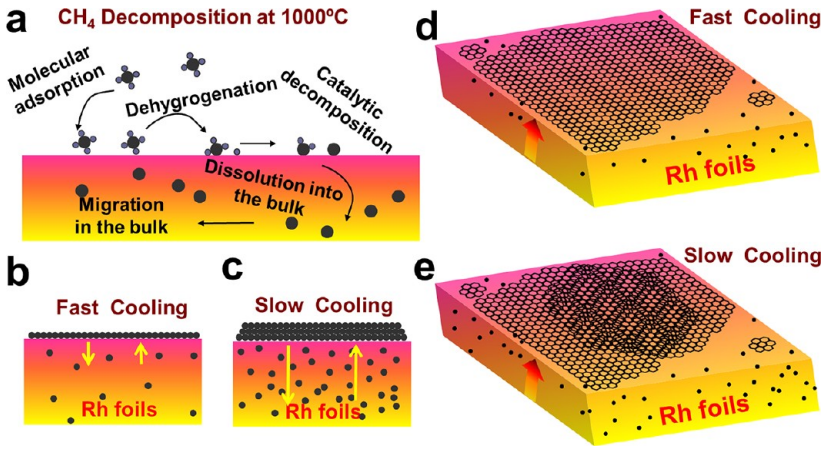

Figure 7. Schematic drawing showing the growth mechanism of graphene on Rh foils. (a) CH_4 decomposition at 1000 °C, followed with carbon dissolution into Rh foils. (b–e) Side-view and 3D images of carbon atoms segregating from bulk to Rh surfaces throughout the quenching processes under fast and slow cooling, forming monolayer and multilayer graphene, respectively.

where the graphene layer thickness distribution *versus* the temperature curve bears three platforms corresponding to multilayer, monolayer graphene, or bare Ni under different growth and cooling processes.[26,27] moiré patterns existing on graphene films are established to be an intriguing phenomenon for segregated graphene. Additionally, high-density wrinkles contribute another unique trait of the system.

CONCLUSION

We have successfully synthesized continuous graphene films on Rh foils by APCVD for the first time and transferred the graphene films onto SiO_2/Si substrate by a bubble method. By changing the cooling rate, we can accurately control the layer number of graphene from monolayer to multilayers. The ubiquitous

On the basis of these results, we propose a segregation mechanism for graphene growth on Rh foils, an analogue of graphene on Ni films because of their high carbon solubility. The fantastic morphology and the versatile stacking order of graphene layers make CVD graphene on Rh foils a perfect system to detect newfangled physical properties such as VHSs in twisted graphene layers.

METHODS

Preparation of Graphene. Poly-Rh substrates (Rh foil, 0.025 mm thick, 99.9% metals basis) were purchased from Sigma-Aldrich. In the growth process, the Rh foil was first heated from room temperature to 1000 °C in 45 min under a H_2 flow of 200 sccm and then kept at 1000 °C for 40 min for deoxidation of the impurity. Later on, 5–10 sccm CH_4 was introduced into the furnace and the gas mixing ratio of CH_4/H_2 could range from 5/700 to 5/200. After that, the sample was cooled with different cooling rates. Due to the inert nature of graphene, the as-grown sample can be loaded out of the growth furnace for further characterizations.

Transferring Graphene from Rh Substrates. As Rh is chemically inert and very expensive, we use a bubble method to isolate graphene films to insulated substrates. The transfer procedure includes the following: (1) spin-coating polymethylmethacrylate (PMMA) film onto the graphene surface; (2) dipping the PMMA/graphene/Rh foil into a 1 mol/L (M) NaOH aqueous solution as a cathode of an electrolysis cell and a platinum wire as an anode, with a 0.2 A constant current supply. The PMMA/graphene layer can be detached from Rh foils since a large amount of H_2 bubbles form between graphene and Rh foil; (3) putting PMMA/graphene film on SiO_2/Si substrates; (4) dissolving PMMA by acetone.

OM, SEM, Raman, TEM, AFM, and STM Characterizations. OM (Olympus BX51), SEM (S-4800), and AFM (Nanoscope IIIa) were used to obtain the graphene domain size and the wrinkle shape and density. AFM images were captured in tapping mode. A Reni Shaw (1000) Raman and a TEM (F20) were used to achieve the thickness of graphene layers. The STM images were captured in an Omicron UHV variable-temperature STM (UHV-VT-STM) with a base pressure better than 10^{-10} mbar. Prior to STM observations, the graphene sample was degassed under UHV conditions for 2 h at 300 °C to remove the impurity adsorptions. All of the STM data were captured under a constant current mode at room temperature.

Conflict of Interest: The authors declare no competing financial interest.

Acknowledgment. This work was financially supported by The Ministry of Science and Technology of China (Grant Nos. 2012CB921404 and 2011CB921903), the National Natural Science Foundation of China (Grant Nos. 21073003 and 51222201), Foundation for Innovative Research Groups of the National Natural Science Foundation of China (Grant No. 51121091), and a foundation for the Author of National Excellent Doctoral Dissertation of PR China (201087).

Supporting Information Available: The schematic of the APCVD temperature progress of graphene growth, and the additional Raman mapping, STM, SAED, SEM, and XPS depth characterizations of graphene on Rh foils. This material is available free of charge *via* the Internet at http://pubs.acs.org.

REFERENCES AND NOTES

1. Novoselov, K. S.; Geim, A. K.; Morozov, S. V.; Jiang, D.; Zhang, Y.; Dubonos, S. V.; Grigorieva, I. V.; Firsov, A. A.

Electric Field Effect in Atomically Thin Carbon Films. *Science* **2004**, *306*, 666–669.
2. Novoselov, K. S.; Jiang, Z.; Zhang, Y.; Morozov, S. V.; Stormer, H. L.; Zeitler, U.; Maan, J. C.; Boebinger, G. S.; Kim, P.; Geim, A. K. Room-Temperature Quantum Hall Effect in Graphene. *Science* **2007**, *315*, 1379–1379.
3. Novoselov, K. S.; Geim, A. K.; Morozov, S. V.; Jiang, D.; Katsnelson, M. I.; Grigorieva, I. V.; Dubonos, S. V.; Firsov, A. A. Two-Dimensional Gas of Massless Dirac Fermions in Graphene. *Nature* **2005**, *438*, 197–200.
4. Zhang, Y. B.; Tan, Y. W.; Stormer, H. L.; Kim, P. Experimental Observation of the Quantum Hall Effect and Berry's Phase in Graphene. *Nature* **2005**, *438*, 201–204.
5. Bae, S.; Kim, H.; Lee, Y.; Xu, X. F.; Park, J. S.; Zheng, Y.; Balakrishnan, J.; Lei, T.; Kim, H. R.; Song, Y. I.; *et al.* Roll-to-roll Production of 30-in. Graphene Films for Transparent Electrodes. *Nat. Nanotechnol.* **2010**, *5*, 574–578.
6. Kim, K. S.; Zhao, Y.; Jang, H.; Lee, S. Y.; Kim, J. M.; Kim, K. S.; Ahn, J. H.; Kim, P.; Choi, J. Y.; Hong, B. H. Large-Scale Pattern Growth of Graphene Films for Stretchable Transparent Electrodes. *Nature* **2009**, *457*, 706–710.
7. Ohta, T.; Bostwick, A.; Seyller, T.; Horn, K.; Rotenberg, E. Controlling the Electronic Structure of Bilayer Graphene. *Science* **2006**, *313*, 951–954.
8. Oostinga, J. B.; Heersche, H. B.; Liu, X. L.; Morpurgo, A. F.; Vandersypen, L. M. K. Gate-Induced Insulating State in Bilayer Graphene Devices. *Nat. Mater.* **2008**, *7*, 151–157.
9. Geim, A. K.; Novoselov, K. S. The Rise of Graphene. *Nat. Mater.* **2007**, *6*, 183–191.
10. Zhang, Y. B.; Tang, T. T.; Girit, C.; Hao, Z.; Martin, M. C.; Zettl, A.; Crommie, M. F.; Shen, Y. R.; Wang, F. Direct Observation of a Widely Tunable Bandgap in Bilayer Graphene. *Nature* **2009**, *459*, 820–823.
11. Castro, E. V.; Novoselov, K. S.; Morozov, S. V.; Peres, N. M. R.; dos Santos, J. M. B. L.; Nilsson, J.; Guinea, F.; Geim, A. K.; Neto, A. H. C. Biased Bilayer Graphene: Semiconductor with a Gap Tunable by the Electric Field Effect. *Phys. Rev. Lett.* **2007**, *99*, 216802/1–216802/4.
12. Li, G. H.; Luican, A.; dos Santos, J. M. B. L.; Neto, A. H. C.; Reina, A.; Kong, J.; Andrei, E. Y. Observation of Van Hove Singularities in Twisted Graphene Layers. *Nat. Phys.* **2010**, *6*, 109–113.
13. Chen, Z.; Yuan, H.; Zhang, Y.; Nomura, K.; Gao, T.; Gao, Y.; Shimotani, H.; Liu, Z. F.; Iwasa, Y. Tunable Spin−Orbit Interaction in Trilayer Graphene Exemplified in Electric-Double-Layer Transistors. *Nano Lett.* **2012**, *12*, 2212–2216.
14. Reina, A.; Jia, X. T.; Ho, J.; Nezich, D.; Son, H. B.; Bulovic, V.; Dresselhaus, M. S.; Kong, J. Large Area, Few-Layer Graphene Films on Arbitrary Substrates by Chemical Vapor Deposition. *Nano Lett.* **2009**, *9*, 30–35.
15. Vivekchand, S. R. C.; Rout, C. S.; Subrahmanyam, K. S.; Govindaraj, A.; Rao, C. N. R. Graphene-Based Electrochemical Supercapacitors. *J. Chem. Sci.* **2008**, *120*, 9–13.
16. Hou, J. B.; Shao, Y. Y.; Ellis, M. W.; Moore, R. B.; Yi, B. L. Graphene-Based Electrochemical Energy Conversion and Storage: Fuel Cells, Supercapacitors and Lithium Ion Batteries. *Phys. Chem. Chem. Phys.* **2011**, *13*, 15384–15402.
17. Li, X. S.; Cai, W. W.; Colombo, L.; Ruoff, R. S. Evolution of Graphene Growth on Ni and Cu by Carbon Isotope Labeling. *Nano Lett.* **2009**, *9*, 4268–4272.
18. Huang, P. Y.; Ruiz-Vargas, C. S.; van der Zande, A. M.; Whitney, W. S.; Levendorf, M. P.; Kevek, J. W.; Garg, S.; Alden, J. S.; Hustedt, C. J.; Zhu, Y.; Park, J.; *et al.* Grains and Grain Boundaries in Single-Layer Graphene Atomic Patchwork Quilts. *Nature* **2011**, *469*, 389–392.
19. Yu, Q. K.; Jauregui, L. A.; Wu, W.; Colby, R.; Tian, J. F.; Su, Z. H.; Cao, H. L.; Liu, Z. H.; Pandey, D.; Wei, D. G.; *et al.* Control and Characterization of Individual Grains and Grain Boundaries in Graphene Grown by Chemical Vapour Deposition. *Nat. Mater.* **2011**, *10*, 443–449.
20. Liu, N.; Fu, L.; Dai, B. Y.; Yan, K.; Liu, X.; Zhao, R. Q.; Zhang, Y. F.; Liu, Z. F. Universal Segregation Growth Approach to Wafer-Size Graphene from Non-noble Metals. *Nano Lett.* **2011**, *11*, 297–303.
21. Zhang, Y.; Gomez, L.; Ishikawa, F. N.; Madaria, A.; Ryu, K.; Wang, C. A.; Badmaev, A.; Zhou, C. W. Comparison of Graphene Growth on Single-Crystalline and Polycrystalline Ni by Chemical Vapor Deposition. *J. Phys. Chem. Lett.* **2010**, *1*, 3101–3107.
22. Zhang, Y. F.; Gao, T.; Xie, S. B.; Dai, B. Y.; Fu, L.; Gao, Y. B.; Chen, Y. B.; Liu, M. X.; Liu, Z. F. Different Growth Behaviors of Ambient Pressure Chemical Vapor Deposition Graphene on Ni(111) and Ni Films: A Scanning Tunneling Microscopy Study. *Nano Res.* **2012**, *5*, 402–411.
23. Reina, A.; Thiele, S.; Jia, X. T.; Bhaviripudi, S.; Dresselhaus, M. S.; Schaefer, J. A.; Kong, J. Growth of Large-Area Single- and Bi-layer Graphene by Controlled Carbon Precipitation on Polycrystalline Ni Surfaces. *Nano Res.* **2009**, *2*, 509–516.
24. Thiele, S.; Reina, A.; Healey, P.; Kedzierski, J.; Wyatt, P.; Hsu, P. L.; Keast, C.; Schaefer, J.; Kong, J. Engineering Polycrystalline Ni Films To Improve Thickness Uniformity of the Chemical-Vapor-Deposition-Grown Graphene Films. *Nanotechnology* **2010**, *21*, 015601/1–015601/8.
25. Yu, Q. K.; Lian, J.; Siriponglert, S.; Li, H.; Chen, Y. P.; Pei, S. S. Graphene Segregated on Ni Surfaces and Transferred to Insulators. *Appl. Phys. Lett.* **2008**, *93*, 113103/1–113103/3.
26. Shelton, J. C.; Patil, H. R.; Blakely, J. M. Equilibrium Segregation of Carbon to a Nickel (111) Surface−Surface Phase-Transition. *Surf. Sci.* **1974**, *43*, 493–520.
27. Odahara, G.; Otani, S.; Oshima, C.; Suzuki, M.; Yasue, T.; Koshikawa, T. *In-Situ* Observation of Graphene Growth on Ni(111). *Surf. Sci.* **2011**, *605*, 1095–1098.
28. Merino, P.; Svec, M.; Pinardi, A. L.; Otero, G.; Martin-Gago, J. A. Strain-Driven Moire Superstructures of Epitaxial Graphene on Transition Metal Surfaces. *ACS Nano* **2011**, *5*, 5627–5634.
29. Gao, J. H.; Sagisaka, K.; Kitahara, M.; Xu, M. S.; Miyamoto, S.; Fujita, D. Graphene Growth on a Pt(111) Substrate by Surface Segregation and Precipitation. *Nanotechnology* **2012**, *23*, 055704/1–055704/5.
30. N'Diaye, A. T.; Bleikamp, S.; Feibelman, P. J.; Michely, T. Two-Dimensional Ir Cluster Lattice on a Graphene Moire on Ir(111). *Phys. Rev. Lett.* **2006**, *97*, 21501/1–205501/4.
31. N'Diaye, A. T.; Coraux, J.; Plasa, T. N.; Busse, C.; Michely, T. Structure of Epitaxial Graphene on Ir(111). *New J. Phys.* **2008**, *10*, 043033/1–043033/16.
32. Coraux, J.; N'Diaye, A. T.; Busse, C.; Michely, T. Structural Coherency of Graphene on Ir(111). *Nano Lett.* **2008**, *8*, 565–570.
33. Coraux, J.; N'Diaye, A. T.; Engler, M.; Busse, C.; Wall, D.; Buckanie, N.; Heringdorf, F. J. M. Z.; van Gastel, R.; Poelsema, B.; Michely, T. Growth of Graphene on Ir(111). *New J. Phys.* **2009**, *11*, 023006/1–023006/22.
34. Hattab, H.; N'Diaye, A. T.; Wall, D.; Klein, C.; Jnawali, G.; Coraux, J.; Busse, C.; van Gastel, R.; Poelsema, B.; Michely, T.; Horn-von Hoegen, M.; *et al.* Interplay of Wrinkles, Strain, and Lattice Parameter in Graphene on Iridium. *Nano Lett.* **2012**, *12*, 678–682.
35. Sutter, P. W.; Flege, J. I.; Sutter, E. A. Epitaxial Graphene on Ruthenium. *Nat. Mater.* **2008**, *7*, 406–411.
36. Sutter, E.; Acharya, D. P.; Sadowski, J. T.; Sutter, P. Scanning Tunneling Microscopy on Epitaxial Bilayer Graphene on Ruthenium (0001). *Appl. Phys. Lett.* **2009**, *94*, 133101/1–133101/3.
37. Pan, Y.; Zhang, H. G.; Shi, D. X.; Sun, J. T.; Du, S. X.; Liu, F.; Gao, H. J. Highly Ordered, Millimeter-Scale, Continuous, Single-Crystalline Graphene Monolayer Formed on Ru (0001). *Adv. Mater.* **2009**, *21*, 2777–2780.
38. Kwon, S. Y.; Ciobanu, C. V.; Petrova, V.; Shenoy, V. B.; Bareno, J.; Gambin, V.; Petrov, I.; Kodambaka, S. Growth of Semiconducting Graphene on Palladium. *Nano Lett.* **2009**, *9*, 3985–3990.
39. Murata, Y.; Starodub, E.; Kappes, B. B.; Ciobanu, C. V.; Bartelt, N. C.; McCarty, K. F.; Kodambaka, S. Orientation-Dependent Work Function of Graphene on Pd(111). *Appl. Phys. Lett.* **2010**, *97*, 143114/1–143114/3.
40. Sicot, M.; Bouvron, S.; Zander, O.; Rudiger, U.; Dedkov, Y. S.; Fonin, M. Nucleation and Growth of Nickel Nanoclusters on Graphene Moire on Rh(111). *Appl. Phys. Lett.* **2010**, *96*, 093115/1–093115/3.
41. Wang, B.; Caffio, M.; Bromley, C.; Fruchtl, H.; Schaub, R. Coupling Epitaxy, Chemical Bonding, and Work Function

at the Local Scale in Transition Metal-Supported Graphene. *ACS Nano* **2010**, *4*, 5773–5782.
42. Sicot, M.; Leicht, P.; Zusan, A.; Bouvron, S.; Zander, O.; Weser, M.; Dedkov, Y. S.; Horn, K.; Fonin, M. Size-Selected Epitaxial Nanoislands Underneath Graphene Moire on Rh(111). *ACS Nano* **2012**, *6*, 151–158.
43. Muller, F.; Sachdev, H.; Hufner, S.; Pollard, A. J.; Perkins, E. W.; Russell, J. C.; Beton, P. H.; Gsell, S.; Fischer, M.; Schreck, M.; *et al.* How Does Graphene Grow? Easy Access to Well-Ordered Graphene Films. *Small* **2009**, *5*, 2291–2296.
44. Preobrajenski, A. B.; Ng, M. L.; Vinogradov, A. S.; Martensson, N. Controlling Graphene Corrugation on Lattice-Mismatched Substrates. *Phys. Rev. B.* **2008**, *78*, 073401/1–073401/4.
45. Chae, S. J.; Gunes, F.; Kim, K. K.; Kim, E. S.; Han, G. H.; Kim, S. M.; Shin, H. J.; Yoon, S. M.; Choi, J. Y.; Park, M. H.; *et al.* Synthesis of Large-Area Graphene Layers on Poly-Nickel Substrate by Chemical Vapor Deposition: Wrinkle Formation. *Adv. Mater.* **2009**, *21*, 2328–2333.
46. Gao, L. B.; Ren, W. C.; Xu, H. L.; Jin, L.; Wang, Z. X.; Ma, T.; Ma, L. P.; Zhang, Z. Y.; Fu, Q.; Peng, L. M.; *et al.* Repeated Growth and Bubbling Transfer of Graphene with Millimetre-Size Single-Crystal Grains Using Platinum. *Nat. Commun.* **2012**, *3*, 1702/1–1702/7.
47. Jung, I.; Rhyee, J. S.; Son, J. Y.; Ruoff, R. S.; Rhee, K. Y. Colors of Graphene and Graphene-Oxide Multilayers on Various Substrates. *Nanotechnology* **2012**, *23*, 025708/1–025708/8.
48. Yan, W.; Liu, M.; Dou, R.-F.; Meng, L.; Feng, L.; Chu, Z.-D.; Zhang, Y.; Liu, Z.; Nie, J.-C.; He, L. Angle-Dependent Van Hove Singularities in a Slightly Twisted Graphene Bilayer. *Phys. Rev. Lett.* **2012**, *109*, 126801/1–126801/5.
49. Zhang, Y. F.; Gao, T.; Gao, Y. B.; Xie, S. B.; Ji, Q. Q.; Yan, K.; Peng, H. L.; Liu, Z. F. Defect-like Structures of Graphene on Copper Foils for Strain Relief Investigated by High-Resolution Scanning Tunneling Microscopy. *ACS Nano* **2011**, *5*, 4014–4022.
50. Zhu, W. J.; Low, T.; Perebeinos, V.; Bol, A. A.; Zhu, Y.; Yan, H. G.; Tersoff, J.; Avouris, P. Structure and Electronic Transport in Graphene Wrinkles. *Nano Lett.* **2012**, *12*, 3431–3436.
51. Arnoult, W. J.; Mclellan, R. B. Solubility of Carbon in Rhodium Ruthenium, Iridium and Rhenium. *Scr. Metall. Mater.* **1972**, *6*, 1013–1018.